Dual-Particle Synergy in Bio-Based Linseed-Oil Pickering Emulsions: Optimising ZnO–Silica Networks for Greener Sunscreens

Marina Barquero , Luis A. Trujillo-Cayado * , Jenifer Santos *

Posted Date: 4 June 2025

doi: 10.20944/preprints202506.0208.v1

Keywords: aerosil; appyclean; linseed oil; nanoemulsion; pickering

 doi:10.20944/preprints202506.0208.v1

Article

Dual-Particle Synergy in Bio-Based Linseed-Oil Pickering Emulsions: Optimising ZnO–Silica Networks for Greener Sunscreens

Marina Barquero [1], Luis A. Trujillo-Cayado [1,*] and Jenifer Santos [2,*]

[1] Departamento de Ingeniería Química, Escuela Politécnica Superior, Universidad de Sevilla, c/Virgen de África, 6, E41007 Sevilla, Spain

[2] Departamento de Ciencias de la Salud y Biomédicas, Facultad de Ciencias de la Salud, Universidad Loyola Andalucía, Avda. de las Universidades s/n, Dos Hermanas, 41704 Sevilla, Spain

* Correspondence: ltrujillo@us.es (L.A.T-C); jsgarcia@uloyola.es (J.S.)

Abstract: The development of mineral, biodegradable sunscreens that can offer both high photoprotection and long-term colloidal stability, while limiting synthetic additives, presents a significant challenge. A linseed-oil nanoemulsion co-stabilised by ZnO nanoparticles and the eco-friendly surfactant Appyclean 6552 was formulated, and the effect of incorporating fumed silica/alumina (Aerosil COK 84) was evaluated. A central composite response surface design was used to ascertain the oil/ZnO ratio that maximized the in vitro sun protection factor at sub-300 nm droplet size. The incorporation of Aerosil at concentrations ranging from 0 to 2 wt.% resulted in a transformation of the dispersion from a nearly Newtonian state to a weak-gel behavior. This alteration was accompanied by a reduction in the Turbiscan Stability Index. Microscopic analysis has revealed a hierarchical particle architecture, in which ZnO forms Pickering shells around each droplet, while Aerosil aggregates bridge neighboring interfaces, creating a percolated silica scaffold that immobilizes droplets and amplifies multiple UV scattering. The findings demonstrate that coupling interfacial Pickering armor with a continuous silica network yields a greener, physically robust mineral sunscreen and offers a transferable strategy for stabilizing plant-oil emulsions containing inorganic actives.

Keywords: aerosol; appyclean; linseed oil; nanoemulsion; pickering

1. Introduction

A nanoemulsion is a dispersed system in which droplets of one phase (usually oily) are dispersed in another phase (usually aqueous) and have an extremely small size, usually in the range of 10 to 300 nanometers. This nanometer size gives nanoemulsions unique physical and functional properties, such as high stability and high specific surface area. The nanometric size of nanoemulsions enables greater absorption of encapsulated compounds into the body due to the enhanced permeability of the cellular and tissue membranes [1]. This is particularly beneficial for lipophilic or low-water-solubility compounds, such as certain vitamins and pharmaceuticals, as the nanoemulsion enhances their dispersion in aqueous solutions and facilitates their absorption into the body [2]. Furthermore, the encapsulation of compounds in nanoemulsions affords protection from external factors such as oxidation, light and heat, which otherwise cause degradation. This is particularly crucial for compounds that are susceptible to degradation, such as antioxidants, essential fatty acids, and certain pharmaceuticals, which are preserved for an extended period under optimal conditions [3]. Because of these properties, the popularity of nanoemulsions as encapsulation systems has gained a lot of attention in the last years, and they can used in a diverse range of applications, notably within the pharmaceutical, cosmetic, and food industries [4].

Flaxseed oil, also known as linseed oil and used in this study as dispersed phase, is obtained from the seeds of the flax plant (*Linum usitatissimum*). It is recognized for its many nutritional

 doi:10.20944/preprints202506.0208.v1

properties and health benefits such as high levels of antioxidants, skin benefits and anti-inflammatory properties, among others [5]. It is a rich source of essential fatty acids, particularly alpha-linolenic acid (ALA), a type of omega-3 that plays a key role in maintaining the integrity of the skin's lipid barrier. This facilitates the retention of moisture by the skin, resulting in a more even, hydrated and healthy appearance. The high omega-3 and antioxidant content of flax oil has been demonstrated to reduce inflammation and soothe the skin, which is beneficial for individuals with conditions such as acne, rosacea, eczema or psoriasis. Furthermore, it has been demonstrated to alleviate swelling and redness in individuals with sensitive or irritated skin [6,7].

In contrast to chemical sunscreens, which absorb UV rays and convert them into heat, zinc oxide functions as a physical blocker or mineral filter. This results in the formation of a layer on the surface of the skin that reflects and scatters UV radiation, thereby preventing its penetration into the skin [8]. This makes it an appropriate choice for individuals with sensitive skin, as it is less prone to causing irritation or allergic [9]. Furthermore, it is one of the few approved ingredients that provides protection against both UVB rays and UVA rays. In addition to its photoprotective effects, zinc oxide has been demonstrated to possess soothing and anti-inflammatory properties, rendering it a beneficial agent for individuals with skin prone to irritation. Furthermore, it has been demonstrated to alleviate redness and inflammation, which is beneficial in the aftermath of sun exposure [10,11].

In order to stabilise nanoemulsions, a surfactant is needed. Appyclean 6552 is a non-ionic surfactant comprising amyl, capryl, and lauryl xylosides derived from wheat. The plant origin of this surfactant ensures its safety, as it is biodegradable and has a low toxicity to the environment (OECD 301F and OECD 311). It has been used before stabilising nanoemulsions and protecting active ingredients from heat and sun [12,13]. In this study, a thickener (Aerosil® COK84) is incorporated into the nanoemulsions to form the cream texture and increase viscosity. Aerosil®COK 84 is a combination of the fumed silica Aerosil®200 and highly dispersed aluminum oxide (AEROXIDE®Alu C) in a 5:1 ratio. It possesses spherical particles in the nanoscale range and it is considered as a thickening and gelling agent [14]. In addition, it has applications in paintings, pharmaceutical, cosmetic and food industry [15–18].

The present study systematically designs and characterises a bio-based linseed-oil nanoemulsion co-stabilised by ZnO nanoparticles and the biodegradable surfactant Aerosil 6552, and subsequently reinforced with fumed silica/alumina. Following a detailed discussion of the materials and preparation protocol, a response-surface methodology is employed to identify the optimal oil/ZnO ratio. This is then followed by an examination of how incremental amounts of Aerosil can be used to tailor the formulation's droplet size distribution, rheology, physical stability and in-vitro SPF. The work elucidates the multiscale mechanism through which ZnO and Aerosil confer synergistic Pickering and network structuring effects by integrating complementary techniques. These techniques include laser diffraction, multiple light scattering, oscillatory rheometry, UV spectrophotometry and FE-SEM. The findings provide both a mechanistic framework and practical guidelines for formulating greener, highly stable sunscreens, thereby bridging the fundamental colloidal principles outlined above with the applied results discussed in the following sections.

2. Materials and Methods

2.1. Materials

Appyclean 6552, a non-ionic and eco-friendly emulsifier, was provided by Wheatoleo (Riom, France). Zinc oxide (ZnO), with a size of less than 5 microns and a purity greater than 99.9%, and Linseed oil were acquired from Sigma-Aldrich (Germany). The solutions were prepared with Milli-Q water, a method that ensures the highest standards of purity and quality. Aerosil® COK 84 was provided by Evonik Industries (Essen, Germany).

2.2. Nanoemulsion Development

 doi:10.20944/preprints202506.0208.v1

The systems were prepared in batches of 50 g with a fixed concentration of Appyclean 6652 of 2.2 wt.%, taking into account a previous study [13]. The continuous phase was prepared by dissolving the surfactant (Appyclean 6552) and the corresponding quantity of zinc oxide (ZnO) in distilled water. The dispersed phase was prepared using the corresponding amount of linseed oil. The development of these linseed oil-in-water emulsions was achieved through a primary homogenization process, which involved the use of an Ultraturrax T25 rotor-stator homogenizer (IKA, Staufen, Germany). This process was carried out semi-continuously, slowly adding the dispersed phase at 8000 rpm for one minute and then 30 seconds at 9000 rpm, operating in discontinuous mode. In order to produce an emulsion with a reduced droplet size (nanoemulsion), the emulsion was subjected to a secondary homogenization process using a VCX750/VCX500 ultrasonic system (Sonics & Materials Inc., USA) with an 830-00427 S-250D acoustic chamber. This process was carried out for a total of 521 seconds, with an amplitude of 75% and pulses of 5:5 s, taking into account the optimum from a previous study [13]. In order to develop an optimal formulation of linseed oil (LO) and zinc oxide (ZnO), variable concentrations were studied using the response surface methodology, as described in the experimental design shown in Table 1.

Table 1. Experimental design used with indication of coded and actual values in weight percentage (wt.%) for the concentration of linseed oil (LO) and zinc oxide (ZnO)

Sample	Linseed oil concentration (LO)	Zinc oxide concentration (ZnO)	Linseed oil concentration (wt.%)	Zinc oxide concentration (wt.%)
1	-1	-1	7.9	1.45
2	1	-1	22.1	1.45
3	-1	1	7.9	8.55
4	1	1	22.1	8.55
5	-1.41	0	5	5
6	1.41	0	25	5
7	0	-1.41	15	0
8	0	1.41	15	10
9	0	0	15	5
10	0	0	15	5

Subsequently, employing the optimal formulation, a rheological modifier (Aerosil® COK 84) was added at 1 and 2 wt.%. The samples were prepared in accordance with the protocol outlined by Trujillo-Cayado et al. (2018) [19].

2.3. Nanoemulsion Characterization

The size distribution of the nanoemulsion droplets was determined at the time of preparation using a Mastersizer 2000 laser diffraction particle size analyzer (Malvern Instruments, United Kingdom). In addition, the Sauter mean diameters ($D_{3,2}$) were determined, which is a way to characterize a dispersed system by linking the total volume of droplets to their surface area. Mathematically, it is the diameter of a sphere that has the same volume-to-surface-area ratio as the entire drop population.

To determine and monitor the physical stability of the samples, multiple light scattering (MLS) measurements were performed in a Turbiscan (Formulaction, France). This non-intrusive method allows destabilization to be identified before it is visible to the naked eye. This method was repeated at different ageing times to assess the stability or instability of the different emulsions over time. In addition, the Turbiscan stability index (TSI) was determined for all samples [20].

The rheological properties of the emulsions were also evaluated one hour after preparation. For this purpose, flow curves and oscillatory tests were carried out using a serrated plate sensor (60 mm diameter, 1 mm separation) and a rotational rheometer model AR2000 (TA Instruments, New Castle,

 doi:10.20944/preprints202506.0208.v1

DE, USA). These tests were carried out at a constant temperature of 25 °C. The samples for FESEM were prepared using a chemical fixation method, according to Vela-Albarrán et al. (2025) [21].

The sun protection factor (SPF) of the test emulsions was assessed in vitro by ultraviolet (UV) spectrophotometry and calculated with the Mansur equation [22]. Briefly, each emulsion was diluted to 1 mg mL^{-1} in ethanol, transferred to a quartz cuvette (1 cm path length), and scanned from 290 to 400 nm at 2-nm intervals with a UV-Vis spectrophotometer. The absorbance (A_λ) values obtained at each wavelength were multiplied by the corresponding erythemal weighting factors (EE_λ) and the solar intensity spectrum (I). SPF was then computed using the expression:

$$SPF = CF \cdot \sum_{290}^{320} EE_\lambda \cdot I_\lambda \cdot A_\lambda \quad (1)$$

where CF = 10 is a correction factor.

2.5. *Statistical Analysis*

To ensure the reliability and reproducibility of the results, all experiments were conducted in triplicate. Standard deviations are represented in the figures as error bars, when observable, or as percentage values in the figure captions. Statistical analysis was performed using one-way analysis of variance (ANOVA) to evaluate the significance of differences among the tested formulations. A confidence level of 95% ($p < 0.05$) was established as the criterion for determining statistical significance. Furthermore, a central composite design (CCD) was utilized to optimize the formulation variables and evaluate their combined effect on the responses of interest. The design, data fitting, and generation of response surface plots were carried out using Echip software (Experimentation by Design, Wilmington, DE, USA). This methodological approach facilitated the identification of optimal processing and compositional conditions through the modeling of the influence of independent variables and their interactions on the measured outputs.

3. Results and Discussion

Figure 1 compares the droplet size distributions of linseed oil nanoemulsions formulated with varying linseed oil and ZnO nanoparticle concentrations. All samples exhibited nanometric droplet sizes; however, it was possible to discern clear trends in the distribution shape and location as a function of composition. It is noteworthy that increasing the linseed oil content results in a shift in the droplet size distribution toward larger diameters and frequently broadens the distribution. For instance, the formulation with the highest oil fraction displays a prominent tail of larger droplets in Figure 1, suggesting the presence of microscale droplets. Conversely, nanoemulsions with reduced oil content yield a more constrained, monomodal distribution, with a concentration of smaller droplets and an absence of substantial, large-droplet tails. Quantitatively, the Sauter mean diameter $D_{3,2}$ demonstrates a marked increase with oil concentration: $D_{3,2}$ increases from approximately 261 nanometers at the lowest oil loading to around 370 nanometers at the highest (see Table 2). This phenomenon can be attributed to the process of agglomeration, wherein larger average droplets are formed when a greater quantity of linseed oil is dispersed, while maintaining a constant ZnO level and energy input. This phenomenon aligns with the principles of emulsion theory and corroborates the findings of previous studies. Specifically, an elevated dispersed-phase fraction tends to generate larger droplets and more extensive size distributions, provided that the surfactant concentration or homogenization energy remains proportionately constant [23]. The presence of larger droplets at elevated oil levels can be ascribed to inadequate emulsifier coverage, which leads to increased coalescence during the emulsification process. This phenomenon results in a diminished total interfacial area and consequently a heightened $D_{3,2}$. In essence, as the linseed oil fraction increases, the emulsification process is unable to maintain the same fine droplet size, resulting in a systematic upward shift in the mean droplet diameter.

Conversely, an increase in the concentration of ZnO nanoparticles results in a decrease in droplet size. Higher loadings of ZnO have been found to be associated with smaller droplet diameters and narrower size distributions in the nanoemulsions. As illustrated in Figure 1, formulations containing

 doi:10.20944/preprints202506.0208.v1

ZnO exhibit a slight shift in their droplet size distributions toward the left, indicating smaller droplet sizes. Additionally, these formulations demonstrate a more pronounced distribution compared to their ZnO-free counterparts. For instance, at a given intermediate oil concentration, the addition of ZnO (at 10 wt.%) has been shown to reduce the peak droplet size and suppress the population of large droplets observable in the tail of the distribution. Consequently, $D_{3,2}$ decreases with increasing ZnO content. For instance, a nanoemulsion containing ZnO (e.g., 5 wt.%) demonstrates a mean droplet size that is smaller than a comparable formulation devoid of ZnO (see Table 2). A modest incorporation of ZnO nanoparticles has been demonstrated to yield a more uniform and finer dispersion of oil droplets, suggesting a potential for enhanced oil dispersion properties. This outcome can be explained by the role of ZnO nanoparticles at the oil–water interface. The ZnO particles likely function as Pickering co-stabilizers, adsorbing at droplet interfaces alongside the surfactant and impeding droplet coalescence. In essence, the nanoparticles provide supplementary steric and/or electrostatic barriers surrounding the droplets, thereby facilitating the formation and stabilization of smaller droplets. As indicated by the extant literature, analogous reductions in droplet size with solid particle additives have been reported in Pickering emulsions. For instance, the addition of sufficient colloidal stabilizers (e.g., cellulose nanofibers or silica) has been shown to yield smaller $D_{3,2}$ values by preventing coalescence and effectively increasing the allowable interfacial area [24,25]. It is noteworthy that in the present system, the ZnO nanoparticles were dispersed in the continuous phase prior to emulsification, ensuring their rapid availability to anchor at newly formed oil–water interfaces. This phenomenon likely contributes to the observed decrease in mean droplet size and the tightening of the size distribution with higher ZnO concentration.

From a scientific and practical perspective, these findings underscore the necessity of achieving an optimal balance in formulation. An elevated oil fraction, if not offset by an adequate amount of surfactant or stabilizer, will result in the production of larger, less uniform droplets. This, in turn, has the potential to compromise the stability of the nanoemulsion. Indeed, larger droplets possess a reduced total surface area and have been shown to accelerate destabilization phenomena such as creaming or coalescence. In contrast, the incorporation of solid nanoparticles, such as ZnO, has been shown to enhance emulsification efficiency and stability through the establishment of a Pickering stabilization effect. This results in the formation of smaller droplets that exhibit greater resistance to coalescence. This outcome is favorable for application goals such as UV-blocking finishes, as smaller droplets and uniform distributions generally result in more stable and transparent formulations. In summary, the droplet size analysis demonstrates a clear correlation with formulation composition: larger oil fractions yield larger average droplets, while higher ZnO nanoparticle concentrations promote smaller and more uniform droplets. The findings, both qualitative and quantitative, demonstrate the efficacy of manipulating the oil-to-surfactant ratio and incorporating inorganic nanoparticles to regulate the size of nanoemulsion droplets (see Figure 1 and Table 2).

 doi:10.20944/preprints202506.0208.v1

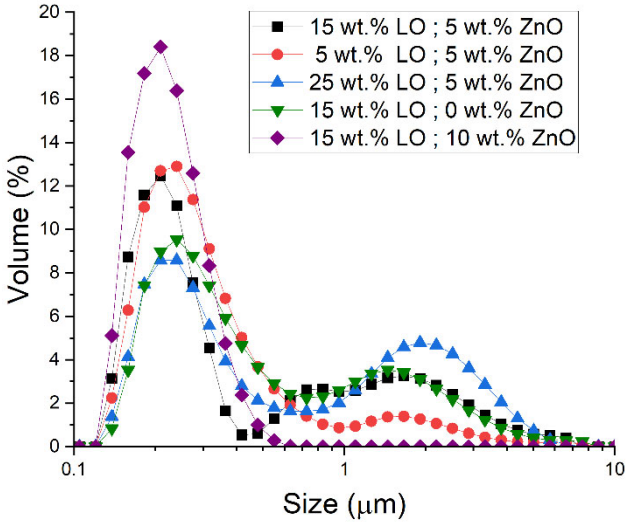

Figure 1. Droplet size distributions of selected nanoemulsions as a function of linseed oil (LO) concentration and zinc oxide concentration (ZnO)

Table 2. Sauter mean diameter ($D_{3,2}$) and sun protection factor (SPF) of the nanoemulsions as a function of the concentration of linseed oil and zinc oxide.

Sample	Linseed oil concentration (wt.%)	Zinc oxide concentration (wt.%)	$D_{3,2}$ (nm)	SPF
1	7.9	1.45	325	2.28
2	22.1	1.45	355	2.45
3	7.9	8.55	259	3.05
4	22.1	8.55	285	3.36
5	5	5	261	2.21
6	25	5	370	2.60
7	15	0	339	0.39
8	15	10	200	3.51
9	15	5	286	2.34
10	15	5	275	2.37

A thorough analysis of the results obtained and presented in Table 2, employing the response surface methodology enables the formulation of an equation ($R^2 = 0.91$) that establishes a correlation between $D_{3,2}$ and the concentrations of linseed oil (LO) and zinc oxide (ZnO):

$$D_{3,2} = 280.4 + 26.3 \cdot LO - 41.6 \cdot ZnO + 21.3 \cdot LO^2 \quad (2)$$

Figure 2 shows the curved, quadratic 2D response surface of the Sauter mean droplet diameter in relation to the concentrations of linseed oil (LO) and zinc oxide (ZnO). The pronounced curvature of the surface indicates that second-order effects are significant and that the relationship is not simply linear. Notably, zinc oxide concentration exerts the largest influence on $D_{3,2}$. Within the explored design window, $D_{3,2}$ decreased monotonically with rising ZnO concentration, and the smallest droplets were obtained at the highest ZnO level tested. No evidence of a plateau or rebound was detected, underscoring that ZnO concentration is the dominant factor governing droplet size in this system, while the LO · ZnO interaction term did not reach statistical significance. A curvature is observed along the LO axis. $D_{3,2}$ increases sharply at high oil loadings due to insufficient stabiliser coverage, but does not drop indefinitely at the lowest LO. Therefore, the response surface trends indicate that moderate oil amounts and the highest concentration of ZnO produce the smallest droplets, whereas excess oil or the absence of ZnO leads to larger $D_{3,2}$ values. According to the

 doi:10.20944/preprints202506.0208.v1

quadratic surface model (Equation 3) and Figure 2, there is a clear optimum region in which the Sauter mean diameter is at its smallest. This optimal point corresponds to Sample 8 in Table 1, which had the smallest $D_{3,2}$ value of all the formulations tested. Sample 8's formulation lies at an intermediate LO concentration and a relatively high ZnO concentration within the design space. In practical terms, this means that using a moderate amount of linseed oil combined with a high level of ZnO nanoparticles produces the finest droplet size. The model predicts a unique minimum rather than a ridge or plateau, indicating that this combination of linseed oil (LO) and zinc oxide (ZnO) is truly optimal for minimizing droplet diameter. Identifying the optimal region for droplet size has important implications for nanoemulsion formulation and stability. Emulsions with a smaller $D_{3,2}$ have slower creaming rates and a lower likelihood of coalescence because the fine droplets have weaker buoyancy (according to Stokes' law) and are more uniformly stabilized.

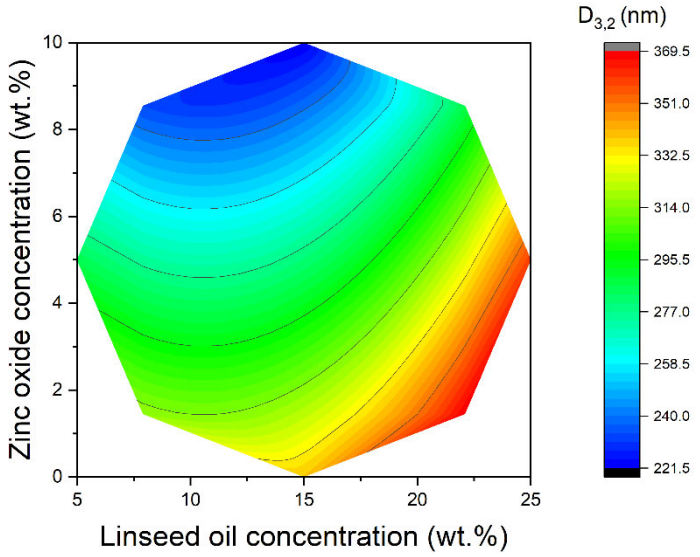

Figure 2. 2D representation of the Sauter mean diameter ($D_{3,2}$) with respect to linseed oil (LO) concentration and zinc oxide concentration (ZnO) according to the quadratic model obtained by the response surface methodology.

The analysis of the results obtained for the Sun Protection Factor (SPF), calculated using Mansur's equation, yielded an equation (R^2=0.92) relating this parameter to the concentrations of linseed oil (LO) and zinc oxide (ZnO):

$$SPF = 2.36 + 0.14 \cdot LO + 0.90 \cdot ZnO \quad (3)$$

As demonstrated in Table 2, within the compositional window that was explored, the in-vitro Sun Protection Factor (SPF) ranges from 0.39 to 3.51. The lowest value recorded (sample 7, LO 15 wt.%, 0 wt.% ZnO) indicates that linseed oil, when applied in isolation, provides only marginal UV screening, consistent with the extant literature which attributes an SPF < 2.0 to most plant oils. Conversely, the introduction of zinc oxide has been demonstrated to raise the SPF in every case; at the same LO level (15 wt.%), the transition from 0 to 5 to 10 wt.% ZnO elevates SPF from 0.39 (sample 7) to 2.34/2.37 (samples 9–10) and finally to 3.51 (sample 8). These increments are consistent with the well-established primary role of micron- or nano-sized ZnO as a broadband physical filter, the efficacy of which is approximately proportional to the volume fraction of particles. Nonetheless, the absolute SPF values remain below those of commercial ZnO creams (typically SPF 15–30 for ≥15 wt.% ZnO), presumably due to the fact that the studied samples are a much simpler formulation [26]. Equation 3 captures these trends with a linear main-effect term for ZnO and a smaller but positive coefficient for LO. The greater magnitude of the ZnO coefficient quantitatively confirms that SPF depends much more strongly on ZnO loading than on the oil phase itself. From a chemical perspective, this outcome is anticipated. ZnO has been demonstrated to attenuate UVA/UVB via two mechanisms: firstly, via scattering, and secondly, via band-gap absorption [27]. In contrast, LO

 doi:10.20944/preprints202506.0208.v1

supplies trace phenolics that absorb weakly in the UVB region. As demonstrated in Figure 3, the fitted surface is characterised by is contours that are almost parallel to the LO axis, but exhibit a steepening gradient with respect to ZnO, thereby underscoring its predominant role. It is evident that a shallow optimum (SPF = 3.5) emerges at an LO of 15 wt.% and a ZnO of 10 wt.%, coinciding with experimental point 8. This is analogous to the optimum for Sauter mean diameter.

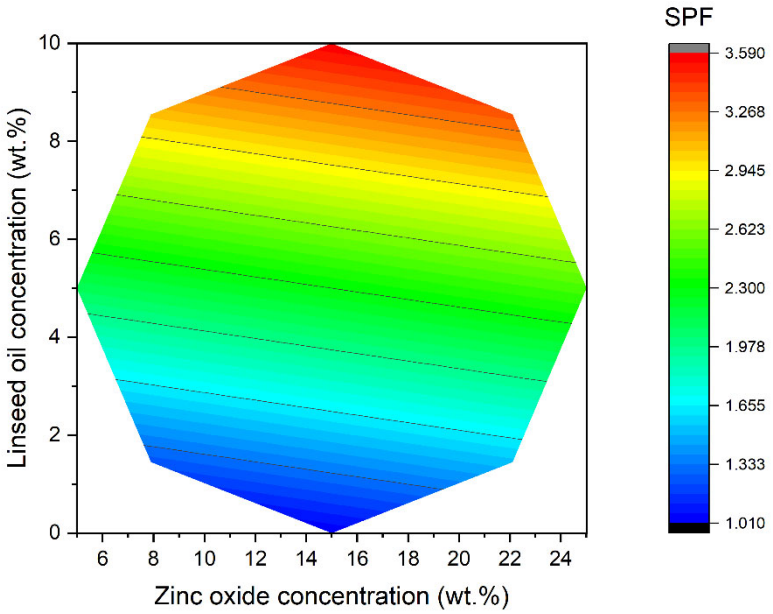

Figure 3. 2D representation of the Sun Protection Factor (SPF) with respect to linseed oil (LO) concentration and zinc oxide concentration (ZnO) according to the quadratic model obtained by the response surface methodology.

The physical stability of the optimal emulsion, formulated with 15 wt.% linseed oil and 10 wt.% zinc oxide, was monitored by multiple light scattering to determine and quantify possible destabilization mechanisms. After seven days, an increase in backscattering was observed in the lower part of the vial, indicating a destabilization mechanism due to the sedimentation of zinc oxide particles. This sedimentation process may be due to the high density of zinc oxide particles compared to the rest of the system and the low viscosity of the emulsion. However, the system showed no signs of destabilization through creaming or coalescence. Thus, the Turbiscan Stability Index (TSI) value for this system was 4.2 ± 0.4 after seven days of ageing. In order to enhance physical stability, modulate rheological properties and augment SPF, Aerosil COK 84 was incorporated into the formulation. Two distinct concentrations were evaluated and compared with the previous optimum (0 wt.% Aerosil COK 84).

The addition of fumed silica/alumina nanoparticle to linseed oil-in-water nanoemulsions containing ZnO has been shown to have a significant effect on the properties of the resultant emulsions. Specifically, an increase in silica concentration has been demonstrated to result in a transformation of rheological and viscoelastic behaviour, alterations to microstructure, and enhancements in physical stability and UV protection performance. These effects are attributed to the ability of Aerosil to establish a particle network within the continuous phase, thereby complementing the roles of oil and ZnO in the formulation.

 doi:10.20944/preprints202506.0208.v1

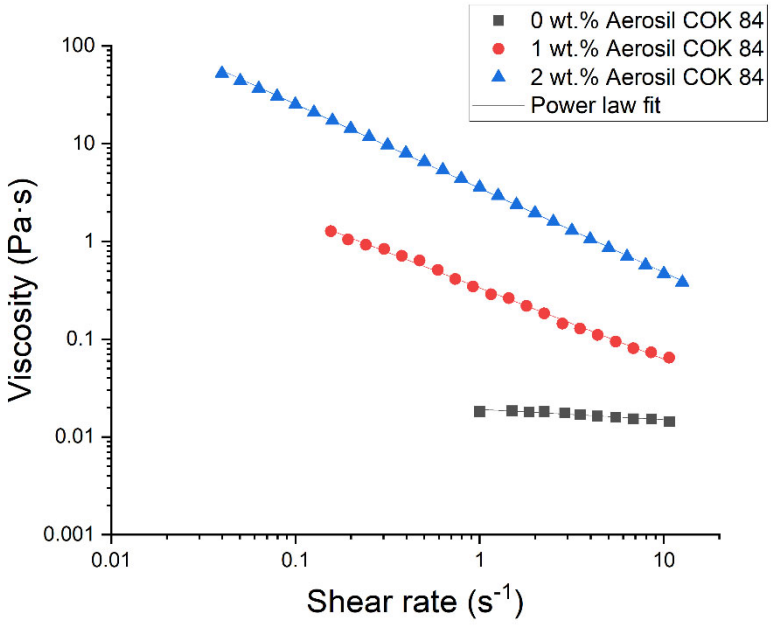

Figure 4. Flow curves of nanoemulsions as a function of Aerosil COK 84 concentration.

The rheological parameters presented in Table 3 demonstrate a distinct, concentration-dependent transition from a nearly Newtonian emulsion to a highly structured, shear-thinning gel. In the absence of Aerosil COK 84, the consistency index k is recorded as 0.019 Pa · s^n and the flow index n is 0.90, suggesting a low-viscosity liquid whose shear stress is nearly proportional to the shear rate. The introduction of 1 wt% Aerosil results in a substantial increase in k, raising it by more than an order of magnitude to 0.334 Pa · s^n. Concurrently, n is reduced to 0.27, indicating the initiation of a three-dimensional particulate network that contributes to yield behaviour and pronounced pseudoplasticity. It is evident that at 2 wt% Aerosil, the network is fully developed, as evidenced by the increase in k to 3.50 Pa·s^n, concomitant with the decrease in n to 0.14. It is evident that the incorporation of varying quantities of Aerosil COK 84 results in significant alterations to the flow behaviour of the nanoemulsions. As demonstrated in Figure 4 and Table 3, an increase in silica levels has been observed to result in elevated viscosity and shear-thinning behavior in emulsions. Even at low shear rates, formulations with high Aerosil content exhibit significantly increased apparent viscosity (often by orders of magnitude) compared to silica-free emulsions. This phenomenon is indicative of the formation of a shear-thinning fluid. This behaviour is indicative of fumed silica dispersions, wherein a three-dimensional network of silica aggregates accumulates at rest and disintegrates under flow. The network is formed from hydrogen bonds and van der Waals attractions between silica particles (and alumina sites), which create a transient gel-like structure in the aqueous continuous phase. Consequently, nanoemulsions with elevated Aerosil concentrations exhibit resistance to flow until a critical shear (yield stress) is attained, at which point they undergo facile flow. This rheology is highly beneficial for product stability and application: the formulation remains thick and prevents phase separation during storage, yet it can be spread easily when rubbed.

Table 3. Consistency index (k), flow index (n), Turbiscan stability Index (TSI) and Sun Protection Factor (SPF) of the nanoemulsions as a function of the Aerosil COK 84 concentration.

Aerosil COK 84 (wt.%)	k (Pa·s^n)	n	TSI	SPF
0	0.0191 ± 0.0003 [a]	0.90 ± 0.01 [a]	4.2 ± 0.4 [a]	3.51 ± 0.08 [a]
1	0.3343 ± 0.0079 [b]	0.27 ± 0.01 [b]	1.3 ± 0.2 [b]	4.00 ± 0.15 [b]
2	3.4978 ± 0.1588 [c]	0.14 ± 0.01 [c]	1.2 ± 0.2 [b]	4.26 ± 0.12 [b]

* standard deviation with statistically significant ($p < 0.05$) difference according to Tukey test.

 doi:10.20944/preprints202506.0208.v1

The oscillatory rheology (Figure 5) further highlights the structural changes induced by Aerosil COK 84. As the silica concentration increases, the nanoemulsion undergoes a transition from a predominantly viscous liquid to a more elastic, solid-like material. It has been demonstrated that with the addition of Aerosil, G′ undergoes a substantial increase that can surpass G″ across a spectrum of frequencies. This phenomenon is indicative of the development of a weak gel structure, characterized by predominant elasticity. The network of silica particles endows the system with the capacity to store elastic energy: under small deformations, the structure resists and recoils (high G′), rather than flowing irreversibly. The emergence of a frequency-independent plateau in G′ at low frequencies for the samples formulated with the fumed silica (as illustrated in Figure 5) is indicative of a percolated network or gel within the sample. Consequently, the loss tangent (G″/G′) decreases with silica content, indicating a transition towards solid-like behavior. These viscoelastic trends are consistent with a particle-bridged droplet network in the emulsions. In this study, it is hypothesized that Aerosil particles in the continuous phase connect via weak bonds and possibly anchor to droplet interfaces, creating an elastic cage that traps the oil droplets. This finding is consistent with reports that the incorporation of colloidal silica into emulsions results in a substantial augmentation of the yield stress and plateau modulus when compared to formulations devoid of silica. It can thus be concluded that Aerosil functions as a structuring agent, thereby converting a purely viscous emulsion into a viscoelastic gel. In contrast, the combination of ZnO and oil alone did not yield the robust gel-like moduli that were observed with silica. It is evident that the supplementation of Aerosil is pivotal in the customization of the linear viscoelastic response.

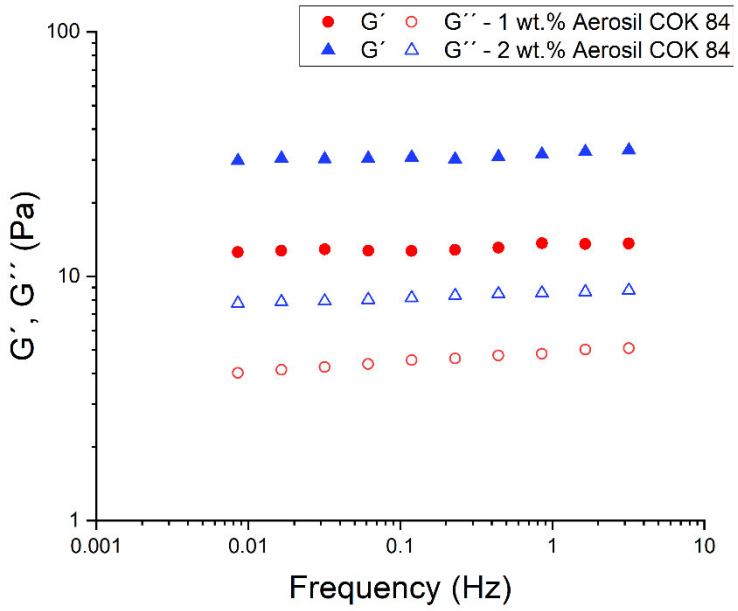

Figure 5. Mechanical spectra as a function of Aerosil COK 84 concentration.

The physical stability of the nanoemulsions, quantified by the Turbiscan Stability Index (TSI) in Table 3, improves markedly with increasing Aerosil content. Conversely, a lower TSI is indicative of reduced phase separation or creaming over time. The data demonstrate that samples devoid of Aerosil exhibit elevated TSI values, indicative of diminished stability. Conversely, samples incorporating Aerosil demonstrate reduced TSI values, suggesting enhanced stability. This enhancement can be directly attributed to the rheological and microstructural effects discussed above. In essence, the arrest of the mobility of droplets and solid particles is induced by silica. Droplet creaming and sedimentation are greatly suppressed because the gel character can counteract the gravitational force on the dispersed particles.

 doi:10.20944/preprints202506.0208.v1

The progressive enrichment of the optimised linseed-oil/ZnO nanoemulsion with Aerosil COK 84 resulted in a measurable enhancement of its photo-protective performance. As demonstrated in Table 3, the in-vitro SPF exhibited an increase with the incorporation of Aerosil, with statistical significance attained at $p < 0.05$. Despite the fact that the absolute gains are modest in comparison to the increase achieved by ZnO itself, they are noteworthy for two reasons. Firstly, the rise occurs without altering either the active ZnO dose or the oil/surfactant ratio, evidencing a genuine synergistic contribution from the fumed silica/alumina particles. Secondly, the incremental SPF is accompanied by markedly lower TSI values and a rheology shift from a nearly Newtonian fluid to a weak-gel network. Collectively, these factors delay sedimentation of ZnO and immobilise droplets, thereby preserving the optical homogeneity that is essential for reproducible UV screening.

Figure 6 provides a direct microstructural comparison between the silica-free nanoemulsion (6A) and its counterpart enriched with 1 wt.% Aerosil COK 84 (6B). In micrograph 6A, the oil droplets are distinctly delineated by a thin, continuous corona of adsorbed ZnO nanoparticles, giving rise to a classic Pickering shell. The individual droplets remain largely isolated, and the inter-droplet spaces appear dark and unfilled, indicating that the particle layer is confined to the oil/water interface. The configuration under discussion stabilizes the dispersion against coalescence. However, the absence of an interconnecting particle scaffold leaves significant voids through which droplets may still migrate under gravity or applied shear. The addition of fumed silica/alumina (6B) transforms this discrete architecture into a densely interconnected network. While ZnO continues to armor each droplet, Aerosil aggregates are now observed to be bridging neighboring interfaces and populating the continuous phase, thereby producing a space-filling, fractal-like skeleton. Such a percolated silica framework immobilizes both droplets and ZnO particles, thereby accounting for the pronounced rise in low-frequency elasticity, the order-of-magnitude jump in consistency index, and the halving of the Turbiscan Stability Index reported elsewhere in the manuscript.

When considered collectively, micrographs 6A and 6B provide confirmation of a two-level Pickering mechanism. At the primary level, ZnO exhibits a tendency to adhere to the oil–water interface, a property that functions to reduce interfacial tension and sterically impede droplet coalescence. In the secondary level, Aerosil aggregates are distributed across the continuous phase, forming interconnected networks with ZnO-coated droplets to produce a cohesive, load-bearing gel. This gel functions to impede both sedimentation and creaming, thereby ensuring the stability and integrity of the system.

 doi:10.20944/preprints202506.0208.v1

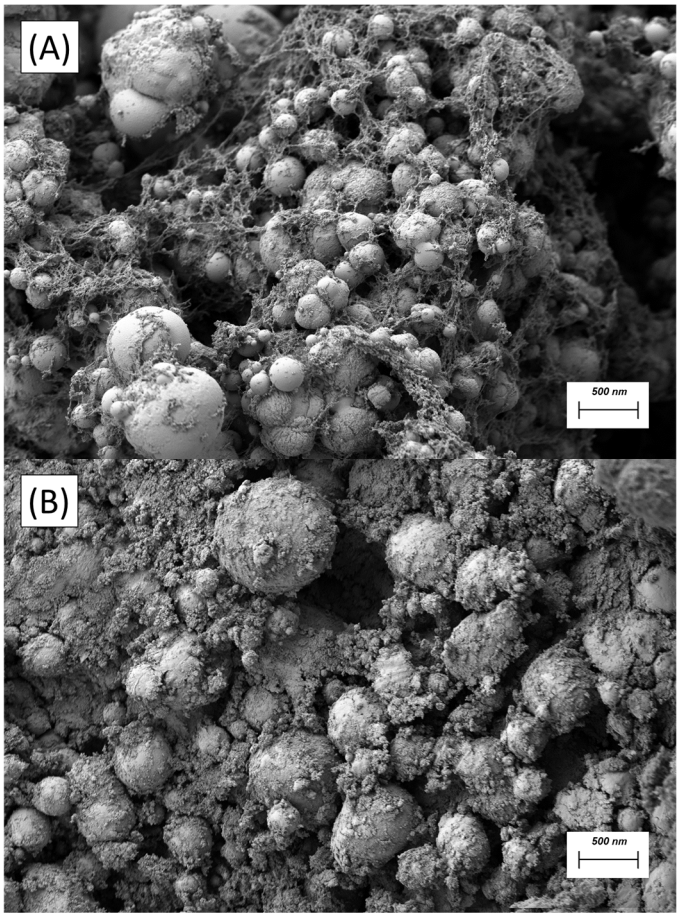

Figure 6. FESEM micrograph of nanoemulsions formulated with 15 wt.% linseed oil, 10 wt.% ZnO and (A) 0 wt.% Aerosil COK 85 and (B) 1 wt.% Aerosil COK 84.

4. Conclusions

The formulation of a linseed-oil/ZnO nanoemulsion in conjunction with the biodegradable surfactant Appyclean 6552 provides a fundamental level of photoprotection, which can be significantly enhanced through the incorporation of trace amounts of fumed silica/alumina. In the first instance, the central composite response surface design was utilized to identify a linseed-oil/ZnO/Appyclean composition that simultaneously minimized mean droplet size (<300 nm) and maximized baseline in vitro SPF (≈3.5). The addition of Aerosil COK 84 in increasing concentrations, from 0 to 2 wt %, results in the transformation of the initially Newtonian dispersion into a weak elastic gel. This process concomitantly causes a halving of the Turbiscan Stability Index and a 21% increase in the in-vitro SPF, without the necessity of additional ZnO. Field-emission SEM analysis confirms a hierarchical architecture, in which ZnO nanoparticles armor individual droplets while percolated silica aggregates bridge neighboring interfaces, immobilizing the dispersed phase and enhancing multiple UV scattering. The dual particle mechanism provides a physicochemical rationale for simultaneously improving stability and photoprotection, offering a transferable, fully mineral route to greener sunscreen formulations based on plant oils.

Author Contributions: Conceptualization, M.B., L.A.T-C. and J.S.; methodology, L.A.T-C. and J.S.; software, L.A.T-C.; validation, J.S.; formal analysis, M.B. and L.A.T-C.; investigation, M.B.; resources, L.A.T-C. and J.S.; data curation, L.A.T-C. and J.S.; writing—original draft preparation, L.A.T-C and J.S.; writing—review and editing, L.A.T-C and J.S.; visualization, M.B.; supervision, L.A.T-C.; project administration, L.A.T-C. and J.S.; funding acquisition, J.S. All authors have read and agreed to the published version of the manuscript.

Funding: This research was funded by Ministerio de Innovación y Ciencia, Ramón y Cajal Programme.

 doi:10.20944/preprints202506.0208.v1

Data Availability Statement: The data that support the findings of this study are available from the corresponding author upon reasonable request.

Conflicts of Interest: The authors declare no conflicts of interest.

References

1. Naseema, A.; Kovooru, L.; Behera, A.K.; Kumar, K.P.; Srivastava, P. A Critical Review of Synthesis Procedures, Applications and Future Potential of Nanoemulsions. *Advances in Colloid and Interface Science* **2021**, *287*, 102318.
2. Ashaolu, T.J. Nanoemulsions for Health, Food, and Cosmetics: A Review. *Environmental Chemistry Letters* **2021**, *19*, 3381–3395.
3. Barradas, T.N.; de Holanda e Silva, K.G. Nanoemulsions of Essential Oils to Improve Solubility, Stability and Permeability: A Review. *Environmental Chemistry Letters* **2021**, *19*, 1153–1171.
4. Ozogul, Y.; Karsli, G.T.; Durmuş, M.; Yazgan, H.; Oztop, H.M.; McClements, D.J.; Ozogul, F. Recent Developments in Industrial Applications of Nanoemulsions. *Advances in Colloid and Interface Science* **2022**, *304*, 102685.
5. Al-Madhagy, S.; Ashmawy, N.S.; Mamdouh, A.; Eldahshan, O.A.; Farag, M.A. A Comprehensive Review of the Health Benefits of Flaxseed Oil in Relation to Its Chemical Composition and Comparison with Other Omega-3-Rich Oils. *European journal of medical research* **2023**, *28*, 240.
6. Nowak, W.; Jeziorek, M. The Role of Flaxseed in Improving Human Health. In Proceedings of the Healthcare; MDPI, 2023; Vol. 11, p. 395.
7. Shim, Y.Y.; Kim, J.H.; Cho, J.Y.; Reaney, M.J. Health Benefits of Flaxseed and Its Peptides (Linusorbs). *Critical Reviews in Food Science and Nutrition* **2024**, *64*, 1845–1864.
8. Smijs, T.G.; Pavel, S. Titanium Dioxide and Zinc Oxide Nanoparticles in Sunscreens: Focus on Their Safety and Effectiveness. *Nanotechnology, science and applications* **2011**, 95–112.
9. Zvyagin, A.V.; Zhao, X.; Gierden, A.; Sanchez, W.; Ross, J.A.; Roberts, M.S. Imaging of Zinc Oxide Nanoparticle Penetration in Human Skin in Vitro and in Vivo. *Journal of biomedical optics* **2008**, *13*, 064031–064031.
10. Gupta, M.; Mahajan, V.K.; Mehta, K.S.; Chauhan, P.S. Zinc Therapy in Dermatology: A Review. *Dermatology research and practice* **2014**, *2014*, 709152.
11. Park, S.J.; Han, H.S. Effects of a Facial Mask Containing Zinc Oxide-Based Cream on Improving Post-Laser Skin Care. *Journal of Cosmetic Dermatology* **2023**, *22*.
12. Santos, J.; Trujillo-Cayado, L.A.; Barquero, M.; Calero, N. Influence of Type and Concentration of Biopolymer on β-Carotene Encapsulation Efficiency in Nanoemulsions Based on Linseed Oil. *Polymers* **2022**, *14*, 4640.
13. Barquero, M.; Sánchez-García, R.M.; Santos, J.; Trujillo-Cayado, L.A. Investigation of Linseed Oil-in-Water Nanoemulsions with an Ecological Surfactant: Interfacial Activity, Stability and Rheological Enhancements. *Journal of Molecular Liquids* **2024**, *415*, 126367.
14. Zhou, J.; Fedkiw, P.S. Ionic Conductivity of Composite Electrolytes Based on Oligo (Ethylene Oxide) and Fumed Oxides. *Solid State Ionics* **2004**, *166*, 275–293.
15. Sadej, M.; Andrzejewska, E. Silica/Aluminum Oxide Hybrid as a Filler for Photocurable Composites. *Progress in Organic Coatings* **2016**, *94*, 1–8.
16. Trujillo-Cayado, L.A.; Santos, J.; Calero, N.; Alfaro-Rodríguez, M.-C.; Muñoz, J. Strategies for Reducing Ostwald Ripening Phenomenon in Nanoemulsions Based on Thyme Essential Oil. *Journal of the Science of Food and Agriculture* **2020**, *100*, 1671–1677.
17. Saienko, N.V.; Bikov, R.A.; Popov, Y.V.; Demidov, D.V.; Younis, B. The Effect of Silicate Fillers on Adhesion and Adhesion Strength Properties of Water-Based Coatings. *Key Engineering Materials* **2020**, *864*, 73–79.
18. Baumgartner, A.; Planinšek, O. Application of Commercially Available Mesoporous Silica for Drug Dissolution Enhancement in Oral Drug Delivery. *European Journal of Pharmaceutical Sciences* **2021**, *167*, 106015.

 doi:10.20944/preprints202506.0208.v1

19. Trujillo-Cayado, L.A.; Santos, J.; Ramírez, P.; Alfaro, M.C.; Muñoz, J. Strategy for the Development and Characterization of Environmental Friendly Emulsions by Microfluidization Technique. *Journal of Cleaner Production* **2018**, *178*, 723–730.
20. Matusiak, J.; Grządka, E. Stability of Colloidal Systems-a Review of the Stability Measurements Methods. *Annales Universitatis Mariae Curie-Sklodowska, sectio AA–Chemia* **2017**, *72*, 33.
21. Vela-Albarrán, M.; Santos, J.; Calero, N.; Carrillo, F.; Trujillo-Cayado, L.A. Phycocyanin-Psyllium Gel Systems: Rheological Insights and Functional Applications in Algae Oil Emulgels. *Food Bioprocess Technol* **2025**, doi:10.1007/s11947-025-03834-5.
22. Mansur, J. de S.; Breder, M.N.R.; Mansur, M.C. d'Ascenção; Azulay, R.D. Determinação Do Fator de Proteção Solar Por Espectrofotometria. *An. Bras. Dermatol* **1986**, 121–124.
23. Dapčević Hadna\djev, T.; Dokić, P.; Krstonošić, V.; Hadna\djev, M. Influence of Oil Phase Concentration on Droplet Size Distribution and Stability of Oil-in-Water Emulsions. *European Journal of Lipid Science and Technology* **2013**, *115*, 313–321.
24. Martins, L.S.; dos Santos, R.G.; Spinacé, M.A.S. Properties of Cellulose Nanofibers Extracted from Eucalyptus and Their Emulsifying Role in the Oil-in-Water Pickering Emulsions. *Waste and Biomass Valorization* **2022**, *13*, 689–705.
25. Bansal, R.; Nair, S.; Pandey, K.K. UV Resistant Wood Coating Based on Zinc Oxide and Cerium Oxide Dispersed Linseed Oil Nano-Emulsion. *Materials Today Communications* **2022**, *30*, 103177.
26. Osterwalder, U.; Hubaud, J.-C.; Perroux-David, E.; Moraine, T.; van den Bosch, J. Sun-Protection Factor of Zinc-Oxide Sunscreens: SPFin Vitro Too Low Compared to SPFin Vivo—a Brief Review. *Photochemical & Photobiological Sciences* **2024**, 1–11.
27. Ginzburg, A.L.; Blackburn, R.S.; Santillan, C.; Truong, L.; Tanguay, R.L.; Hutchison, J.E. Zinc Oxide-Induced Changes to Sunscreen Ingredient Efficacy and Toxicity under UV Irradiation. *Photochemical & Photobiological Sciences* **2021**, *20*, 1273–1285.